Global and Planetary Change 220 (2023) 104017

Contents lists available at ScienceDirect

Global and Planetary Change

journal homepage: www.elsevier.com/locate/gloplacha

Permafrost controls the displacement rates of large unstable rock-slopes in subarctic environments

I.M. Penna [a,*], F. Magnin [b], P. Nicolet [a,c], B. Etzelmüller [d], R.L. Hermanns [a,e], M. Böhme [a], L. Kristensen [c], F. Nöel [a], M. Bredal [a], J.F. Dehls [a]

[a] Geological Survey of Norway, Trondheim 7491, Norway
[b] EDYTEM Lab, Université Savoie Mont Blanc, CNRS, Le Bourget-du-Lac, 73370, France
[c] The Norwegian Water Resources and Energy Directorate (NVE), Trondheim 7030, Norway
[d] Department of Geosciences, University of Oslo, Oslo 0316, Norway
[e] Department of Geoscience and Technology, Norwegian University of Science and Technology, Trondheim 7031, Norway

ARTICLE INFO

Editor: Dr. Jed O. Kaplan

Keywords:
Subarctic
Permafrost thawing
Unstable rock-slopes
Displacement rates

ABSTRACT

Determining the link between permafrost and the displacement rates of large unstable rock-slopes (LURSs) is fundamental for understanding future hazard scenarios and establishing appropriate management strategies. From an inventory of >500 LURSs in Norway, we investigate the controls of those with available information on their displacement rates (299 LURSs), presenting the first statistical evidence of permafrost as the main driver of displacement rates of LURSs. The probability for a LURS to displace if permafrost is present now or was during the Little Ice Age (LIA) is around 2.1 times higher than if permafrost was already absent during the LIA. This probability is 1.5 times higher for LURSs with current permafrost than for LURSs with permafrost during the LIA that has since melted. Therefore, our findings enrich the classical conception that warming of permafrost increases displacement rates of LURSs, by showing that the complete thawing of permafrost can result in a decrease in displacement rate or even a complete halt of displacement.

1. Introduction

Currently, permafrost underlays ca. 17% of the Earth's land surface and ca. 15% of the land surface area in the Northern Hemisphere (Obu et al., 2019). Throughout the Holocene, its extent has fluctuated significantly, from a minimum areal distribution at the Holocene Thermal Maximum to a maximum expansion during the Little Ice Age (LIA) (Kondratjeva et al., 1993; Lilleøren et al., 2012). Its current warming and thawing at a global scale (Biskaborn et al., 2019) has a number of environmental impacts both globally – such as the release of greenhouse gasses –and locally – for example, in alpine and high-latitude settings by affecting the stability of slopes (Haeberli et al., 1997; Gruber et al., 2004; Lewkowicz and Harris, 2005; Huggel et al., 2012; Swindles et al., 2015; Liljedahl et al., 2016; Hjort et al., 2018; Lewkowicz and Way, 2019).

In the last two decades, permafrost degradation has been found responsible for the occurrence of rock-slope collapses in the Alps, with volumes ranging from thousands to hundreds of thousands of cubic meters (Gruber et al., 2004; Allen et al., 2009; Ravanel and Deline, 2011; Ravanel et al., 2017). For failures of that scale, the relation between the collapse and the degradation of the permafrost has been established at a regional scale. However, for large rock-slope collapses, with volumes of several hundreds of thousands or millions of cubic meters of rocks, any causal relationships that have been proposed up to date are based upon a single or a small number of event investigations (Haeberli et al., 1997; Fischer et al., 2010; Phillips et al., 2017; Svennevig et al., 2020; Shugar et al., 2021), theoretically proposed in mechanical models and evaluated in laboratory experiments (Krautblatter et al., 2013), or have been modelled with a numerical stability model, reproducing the mechanical response of rock-slopes to permafrost degradation (Mamot et al., 2018). A step forward in the global understanding of permafrost degradation as the first control of rock-slope deformation was made in a recent work combining thermal ground conditions with paleo-slip rates of six unstable rock-slopes (Hilger et al., 2021). This work postulated that the frequency of slope failures could increase under warming conditions. But is the relationship so straightforward? Answering this question has implications for understanding landscape evolution and geohazard scenarios and establishing appropriate development strategies in high-mountain settings and arctic and subarctic regions. Norway, with

* Corresponding author.
E-mail address: ivanna.penna@ngu.no (I.M. Penna).

https://doi.org/10.1016/j.gloplacha.2022.104017
Received 11 May 2022; Received in revised form 31 October 2022; Accepted 7 December 2022
Available online 9 December 2022

>500 LURSs identified through a vast program for systematically mapping large unstable rock-slopes (LURSs; Fig. 1; Blikra et al., 2006; Hermanns et al., 2013), and with current and past permafrost conditions covering large part of its territory (Lilleøren et al., 2012; Gisnås et al., 2016a; Magnin et al., 2019), is a perfect natural laboratory to build into this knowledge. Our study statistically explores the link between permafrost and displacement rates of LURSs, by combining ground surface deformation rates determined from satellite remote sensing for all of Norway (Dehls et al., 2019) and in-situ measurements, with modelled current and past ground thermal conditions (Magnin et al., 2019; Gisnås et al., 2016b). Furthermore, the study expands the debate on how landslide hazards in current permafrost areas might change with warmer climate conditions.

2. Methodology

2.1. Characterisation of large unstable rock-slopes

In this work we analyse 509 LURSs with volumes larger than 100,000 m^3. These were identified, mapped and monitored by the Geological Survey of Norway (NGU) through a national program mandated by The Norwegian Water Resources and Energy Directorate (NVE), which started in 2007 (Fig. 1; Oppikofer et al., 2015). Their identification was conducted by using high-resolution (1-m or better) aerial photos and digital elevation models (DEM) and the use of a full national satellite-based ground motion service (http://insar.ngu.no). The assessment of LURSs carried out by NGU includes field mapping, structural and kinematic analyses, monitoring of displacement rates, and in some cases, the dating of sliding surfaces.

In this work, we computed the average orientation of each LURS using the 10 m DEM of Norway and the perimeter of the LURS. We derived the aspect and slope from the DEM (geodesic method) in ArcMap and used these inputs to calculate the normal vector in each cell of the DEM. We then computed a weighted sum of all the normal vectors inside each LURS's polygon. We used the inverse of the cosine of the slope to weight the sum since sloping cells of a DEM represent a larger surface area. Finally, the aspect and slope of the surface represented by the resulting normal vector was computed.

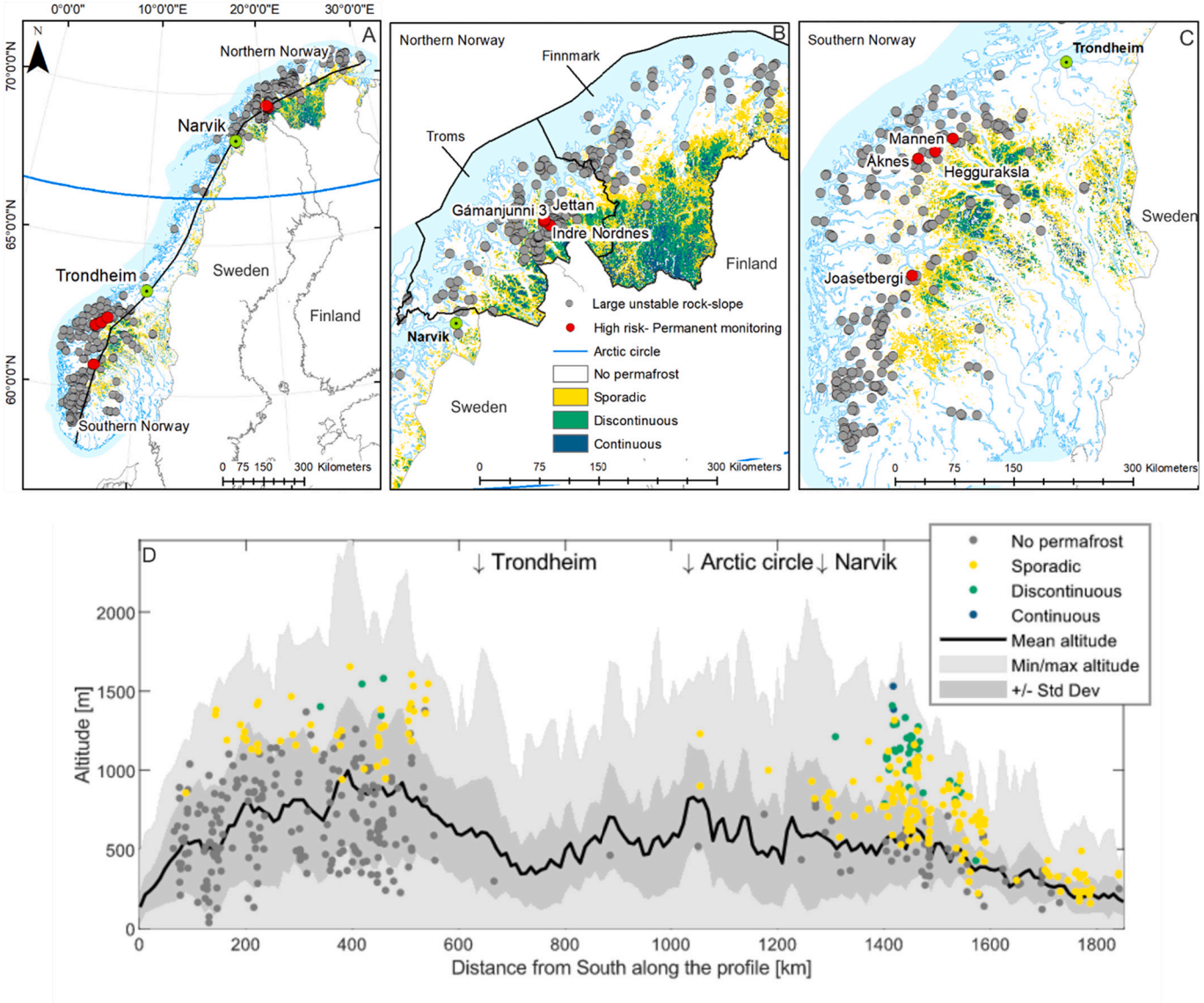

Fig. 1. Observation of LURSs and distribution of permafrost on the mainland of Norway. A) Location of LURSs and type of permafrost (combined from Gisnås et al., 2016a and Magnin et al., 2019). The black line corresponds to the profile displayed in Fig. D. B) Location of LURSs and type of permafrost in northern Norway with indication of extension of Troms and Finnmark counties. C) Location of LURSs and type of permafrost in southern Norway. D) Topographic profile from south to north with locations of LURSs, classified by class of permafrost.

Once the orientation was calculated for each LURS individually, we calculated the average orientation of all the LURSs in a region. To achieve this, we derived a horizontal unit vector from the previously calculated average aspect of each LURS and then the sum all those vectors. If the LURSs are all oriented in the same direction, the resulting vector will be long, while if they are randomly distributed, this vector will be short. To measure this, we computed the strength of the resulting vector (or mean resultant length), which is defined as its length divided by the number of vectors summed (Borradaile, 2003). Thus, a value of 1 means that all the vectors have the same orientation, while a value close to 0 reflects the absence of preferential orientation.

We calculated the LURSs' volumes using the sloping local base-level (SLBL) method (Jaboyedoff et al., 2020), which is an iterative method considering that the volume above a sloping surface connecting the surrounding points, in this case the limits of the instability, can be eroded. A tolerance can be used to create a curved surface, and the value of the tolerance controls the curvature. We implemented this method in an ArcGIS toolbox (https://github.com/ngu/pySLBL). The developed tool calculates the tolerance automatically for each LURS by drawing a profile going through the center of the LURS's polygon and following the average slope direction. The horizontal length (l) of the LURS and its altitude difference (Δz) along this profile are used to estimate the tolerance (c) using the following formula:

$$c = 2 \bullet \left(1 - \sqrt{2}\right) \bullet \Delta z \bullet \left(\frac{x^2}{l^2}\right)$$

where x is the cell size of the DEM. This formula builds on Oppikofer et al. (2016), who propose a method to calculate the minimum, intermediate and maximum tolerance. Since the formula proposed for the intermediate tolerance is not applicable at country scale, we used the formula presented above which corresponds to half of the maximum tolerance of Oppikofer et al., 2016. From our experience, the tolerance as calculated in our study, which is close to the intermediate tolerance of Oppikofer et al. (2016), can be considered acceptable. The volume is given by the difference between the original DEM and the resulting DEM after applying the SLBL method, which represents the thickness of the LURS. The sum of all the pixels of the raster of thickness, multiplied by the area of a pixel, results in the volume of the LURS.

2.2. Measurement of displacement rates

Displacement rates of 299 out of 509 LURSs have been used in this work. Displacement rates were extracted from the NGU database and own measurements using InSAR Norge portal. We used the displacement rates that are representative of entire LURSs, not of single scenarios. Within the framework of the hazard classification system done by NGU (Hermanns et al., 2012), six classes of displacement have been defined: 1. Not significant; 2. <0.5 cm/y; 3. 0.5–1 cm/y; 4. 1–4 cm/y; 5. 4–10 cm/y; and 6. >10 cm/y. LURSs with unknown displacement rates are located mainly on slopes with dense vegetation coverage, are in shadow zones of the Sentinel-1 satellites or are on inaccessible slopes.

The methods used for the monitoring of displacement rates are as follows:

Differential Global Navigation Satellite System (dGNSS): used to measure displacement rates on 95 LURSs. The time the LURSs have been monitored is variable, the longest monitored period with this method spans from 2003 to 2018, and the time interval between the measurements depends on the degree of activity of each LURS, accessibility, and estimated risk, among other factors. The measurements rely on the installation of a network of one or several fixed points in stable outcrops and several points on the unstable rock-mass. GNSS antennas are mounted for each acquisition campaign on bolts fixed to the rocks. Static phase measurements are performed with an interval of a minimum of one year between acquisitions. The measurements are then post-processed using the fixed point(s) as reference. The displacement rate of the LURSs is considered significant if both the following conditions are met:

- the displacement rate obtained by linear regression (v) is higher than the average measurement accuracy (σ_{tot}) multiplied by the square root of two and divided by the time interval between the first and the last measurement (Δt) in years:

$$v > \frac{\sqrt{2} \bullet \sigma_{tot}}{\Delta t}$$

- the displacement follows a coherent trend over at least three measurements.

Tape extensometers: used on 34 LURSs. Here, eye bolts are mounted on both sides of a structure (scarp, crack, etc.), permitting the installation of the instrument at the same location for each acquisition. Repeated measurements are performed with an interval of at least a year. The displacement rates are given by the change of the length of the tape over the years. As for the GPS, a coherent trend shown by at least three measurements (i.e. at least 2 years between the first and last measurement) is necessary to consider the measured velocity reliable.

Interferometric Synthetic Aperture Radar (InSAR): compares microwave images acquired at different times, allowing the detection of surface displacement rates down to mm/y scale, by analysing changes in the phase of the returned microwave (Massonnet and Feigl, 1998). The monitoring can involve both satellite-based InSAR and ground-based InSAR (GB-InSAR) (Wasowski and Bovenga, 2014; Bertolo, 2017; Kristensen et al., 2021).

Satellite InSAR measurements (freely available at https://insar.ngu.no) are based on Sentinel-1 images acquired from 2015 to 2021 and processed with the persistent scatterers method (Ferretti et al., 2000; Ferretti et al., 2001). Sentinel-1 has a spatial resolution of 5 by 20 m, a swath width of 250 km, and a revisit period of either 6 or 12 days between acquisitions. The measurements are one-dimensional along the radar line-of-sight (LOS) and depend on the acquisition geometry. Thus, the accuracy of the method depends on the angle formed by the LOS of the sensor and the vector of displacement of the LURS.

The LOS of the satellites is inclined either towards the west or the east. Therefore, LURSs with stronger northward or southward displacement will have their rates underestimated, but the vertical component will be measured anyhow. The larger the angle between the displacement vector of a LURS and the LOS of the satellite, the more we underestimate the real displacement of a LURS. However, since we are mostly interested in the magnitude of the displacement, the measurements (divided in classes) are acceptable approximations of real displacement rates, but there remains a risk of classifying some LURSs in a lower class of displacement. Because snow coverage hinders the measurements in winter, 2 m-high corner reflectors have been installed on 23 LURSs to allow for measurements throughout the year.

Ground-Based InSAR has been used on 9 LURSs by The Norwegian Water Resources and Energy Directorate (NVE). The measurements were computed along the LOS of a radar mounted to the ground, typically in front of and below the LURS. This makes the instrument's LOS as parallel as possible to the expected displacement vector. The LiSALab radar system is used, which measures in the Ku band, with a central frequency of 17.2 GHz. The instruments can measure displacements exceeding 1 m/day, but since for some LURSs the displacements range from a few mm to a few cm per year, periodic campaigns (about a week in length) are conducted two or more times in a season or over a few years. These campaigns are averaged to a single radar image, and the change of distance between the campaigns is calculated. If a LURS has a very fast displacement, its rate is measured on a daily basis.

2.3. Steep slopes permafrost mapping

To assess current permafrost conditions on LURSs, we extracted the minimum mean annual rock-surface temperature (MARST) value inside the polygon representing each LURS and the corresponding permafrost class (sporadic, discontinuous, continuous) from the 10 m resolution CryoWALL map from Magnin et al. (2019), covering all slopes >40° (fig. S1). When more than one class of permafrost is present, we assign the one covering the largest area. For LURSs in gentler slopes, we assigned the class of permafrost using the regional permafrost model and MAGT temperatures from Gisnås et al. (2016b); this was the case for ca. 10% of the LURSs.

The MARST map derives from a multiple linear regression model, with mean annual air temperature (MAAT) and potential incoming solar radiation (PISR) as explanatory variables. Magnin et al. (2019) calibrated it with in-situ measurements (85 MARST measurement points), local MAAT records and computed PISR at each measurement point using GIS tools. The predicted MARSTs and their standard deviation were used to calculate a permafrost probability (probability that MARST is ≤0 °C), and later converted into a map of permafrost classes, with sporadic permafrost designating areas with permafrost probability of 10 to 50%, discontinuous permafrost designating areas with probability ranging from 50 to 90% and continuous permafrost referring to areas with a probability of >90% (Magnin et al., 2019). Thus, "sporadic permafrost" indicates conditions where permafrost may be very patchy and subsists because of transient effects from past colder climates or because of locally favourable conditions (such as fractured outcrops with air ventilation); "discontinuous permafrost" indicates more widespread areas, but with permafrost temperatures closer to 0 °C, while "continuous permafrost" indicates conditions favourable to permafrost persistence independent of ground characteristics (fractured or not) or debris/snow cover. A probability of 50% corresponds to a MARST of 0 °C.

For this study, we produced MARST and permafrost class maps for the Little Ice Age (LIA; ca. 250 y BP) using the air temperature coefficient of the multiple linear regression model (1.06) and the LIA known air temperature anomaly (compared to the 1961–1990 period). For the LIA anomalies, we used the value −1.5 °C, which is considered to be a reasonable value based on various studies in the wider North-Atlantic region (e.g. Lilleøren et al., 2012; Etzelmüller et al., 2020). As a first step, the air temperature difference was calculated from the periods 1981–1990 and 1961–1990 from the SeNorge air temperature maps and applied to the CryoWALL map (Magnin et al., 2019). Then, we considered the LIA for back analysis and its respective air temperature anomaly of −1.5 °C. For the LIA period, specific MARST, permafrost probability and permafrost class maps were created and used to determine permafrost conditions on LURSs on steep slopes. For LURSs on gentler slopes, the presence of permafrost during LIA was evaluated using the map of Lilleøren et al. (2012) who modelled the distribution of Holocene permafrost in Norway. Fig. S1 shows an example of the MARST map and permafrost maps for the LIA and current times (CT) for a LURS from northern Norway.

2.4. Statistical analyses

We performed statistical analyses to investigate the relation of different variables, namely permafrost, minimum temperature, slope, area and lithology, with the displacement rates of LURSs. Other aspects such as the structural control or the glaciation history where not considered as they are difficult to investigate at such a scale. To further identify if the considered variables are spatially related, the analyses were done for the entire country, the South, the North, and two specific regions of the North: Troms and Finnmark (Fig. 1). Thus, the groups are not independent since Troms and Finnmark are included in the North, which, together with the South, are included in the entire country. Because of the different nature of the studied variables (Table 1), various tests were performed.

Table 1
Tested variables and corresponding data types.

Variable	Type
LIA-CT permafrost	Categorical ordinal
CT permafrost	Categorical ordinal
Min MARST	Interval
Displacement rate	Categorical ordinal
Area	Ratio
Rock type	Categorical nominal
Slope	Ratio

Note: The LIA-CT permafrost is a combination of two ordinal scales. We sorted the classes first by CT and then by LIA to use the combination scale as an ordinal scale, which allows calculating Kendall's τ. Displacement rate is considered on a categorical scale since the available displacement data does not always allow accurate measurement of the displacement rate.

The Chi-squared method (Pearson, 1900) is applied here when both variables are categorical. The observed Chi-squared is given by:

$$X^2 = \sum_{i=1}^{n} \frac{(O_i - E_i)^2}{E_i} \quad (1)$$

where O_i is the observed number of events in class i and E_i is the expected number of events in the same class assuming no correlation (null hypothesis). The p-value is then calculated from the Chi-squared distribution using the corresponding degrees of freedom, calculated as follows:

$$dof = (m-1)^*(n-1) \quad (2)$$

where m and n are the number of classes for the two parameters, respectively. The p-value gives the probability for the Chi-squared, assuming the null hypothesis, to be higher than the observed Chi-squared. Thus, the lower the p-value, the less likely the data is to fulfil the null hypothesis. It is commonly considered that the null hypothesis is rejected for p-values below 0.05 (Borradaile, 2003), which implies that the alternative hypothesis (i.e., that the variables are correlated) is then accepted. Here, we considered the correlation to be significant for p-values below 0.01, partly significant for p-value between 0.01 and 0.1 and not significant for p-values above 0.1. It is recommended to apply the Chi-squared method only when the expected number of events is at least 5 for each class (Borradaile, 2003). Here we classify the velocities in fewer classes (no movement, significant movement <1 cm/y, >1 cm/y) to avoid having classes with too few values, and only use the classes of the other parameters (rock type or permafrost type) when there are at least ten values in them. Even when using fewer classes, we do not always reach the minimum expected value of 5 events in each class, so we present the minimum expected value as a control so that the analyses where this threshold is not reached can be interpreted more carefully (Table S1).

Kendall's τ calculates the association between two rankings. It is calculated from the following equation:

$$\tau = \frac{C - D}{\sqrt{\left(\frac{n(n-1)}{2} - T_x\right)\left(\frac{n(n-1)}{2} - T_y\right)}} \quad (3)$$

where C is the number of concordant pairs, D the number of discordant pairs, n the number of data points, T_x the number of ties on x and T_y the number of ties on y (Agresti, 2010). A concordant pair is a pair (x_1, y_1) and (x_2, y_2) where either $x_1 > x_2$ and $y_1 > y_2$ or $x_1 < x_2$ and $y_1 < y_2$. Kendall's τ takes a value between −1 and 1, where −1 indicates a perfect monotonically decreasing relation, 1 indicates a perfect monotonically increasing relation and 0 indicates the absence of relation. Again, we calculated a p-value, to test for the hypothesis that the two variables do

not show a statistical correlation. Although the p-value, which is two-sided, differs from the one obtained using the Chi-squared method, they can be interpreted similarly. This test is applied without filtering or reclassification since it is not influenced by the number of values in a class.

3. Results

3.1. Distribution of LURSs

LURSs are spatially concentrated in southern Norway (263) and north of the Polar Circle (246; Fig. 1). At a country scale, the median maximum altitude of the headscarps is ca. 700 m a.s.l. (Fig. 2A), although higher in the south than in the north. The spatial distribution of

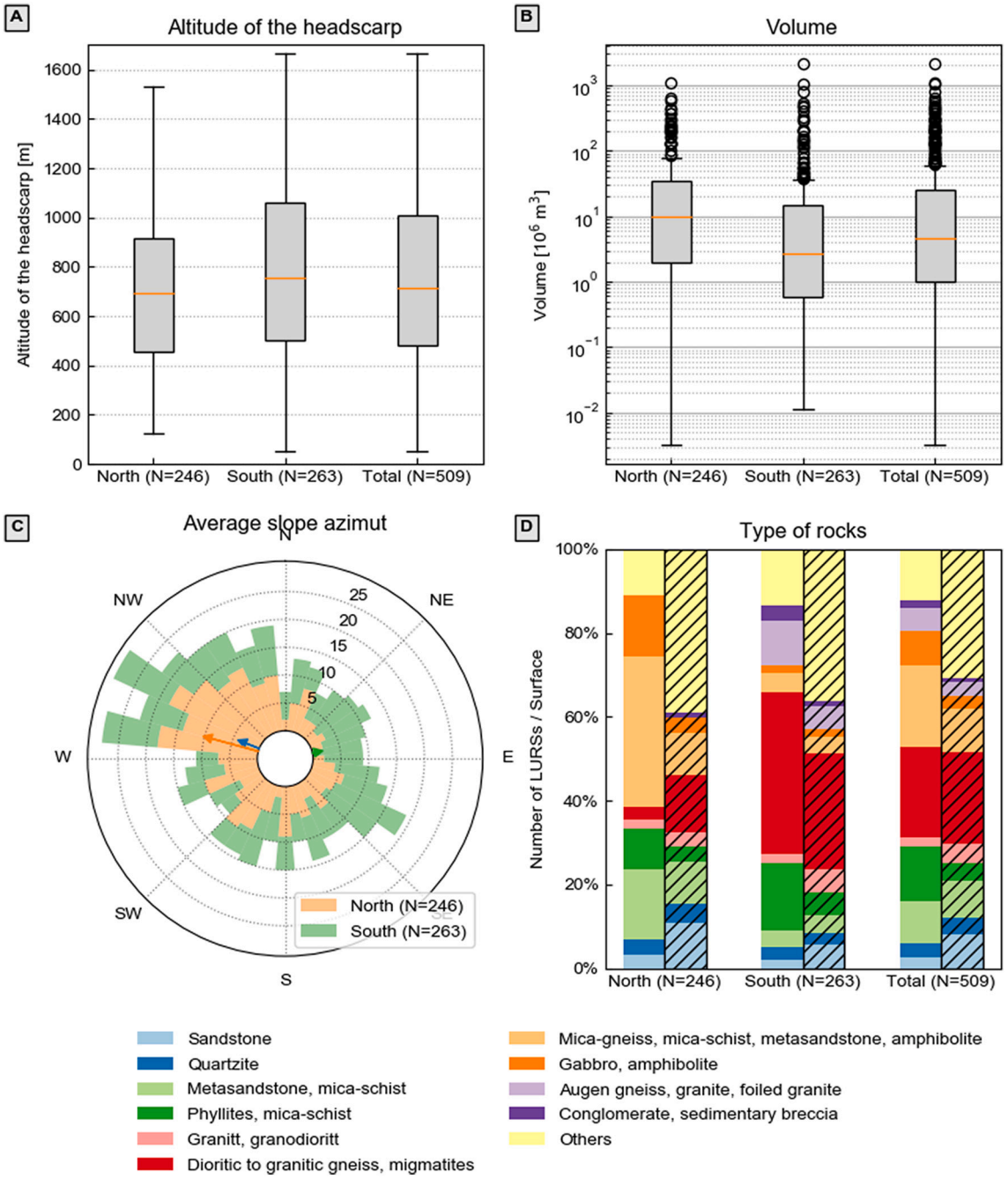

Fig. 2. Characteristics of the LURSs. A) Boxplot with altitude of headscarps per region and for the entire country. B) Boxplot with volume of LURSs per region and for the entire country. C) Rose diagram with the distribution of slope aspects at which LURSs developed. The vectors indicate an eventual preferred orientation, where the vector's length is proportional to its strength. The blue vector is for the whole of Norway; the orange and green are for the North and South respectively. The few LURSs from central Norway are shown as an independent class for completeness but are otherwise only included in the total. D) Stack bar showing the distribution of LURSs by lithologies, and the proportion of the surface covered by those lithologies in the same regions (with hashed pattern). Lithologies were taken from the 1:250000 harmonized bedrock map database (http://geo.ngu.no/kart/berggrunn_mobil/). Note: Boxes in boxplot represent 25–75% quartiles and whiskers are 1.5 interquartile ranges from the median. Medians are shown as orange lines. (For interpretation of the references to colour in this figure legend, the reader is referred to the web version of this article.)

LURSs is associated with geologic and landscape conditions and the Quaternary history. LURSs in southern Norway developed mostly in over-deepened valleys and fjords, and those in northern Norway mainly developed in coastal cliffs carved on flat or gentle relief in Finnmark and in over-deepened valleys and fjords in Troms. The median volume of LURSs in northern Norway is 9.3 * 10^6 m^3 and 2.9 * 10^6 m^3 in the South (Fig. 2B). The mean orientation of LURSs is 291° (WNW) with a vector strength of 0.14, indicating a weak preferential orientation (Fig. 2C; fig. S2). This is mostly influenced by the LURSs in the North (with a preferential orientation of 285° and a vector strength of 0.34), while there is almost no preferential orientation in the South (with a preferential orientation of 78° and a vector strength of 0.06). 82% of LURSs have preferentially developed on five lithologic units, as observed in Fig. 2D. In the North, most LURSs developed on 1) mica-gneisses, mica-schist, metasandstone and amphibolite, while a minor proportion developed on 2) metasandstones and mica-schist. The high proportion of LURSs in unit 1 (35%) is not representative of the distribution of lithologies in this region in which this unit is only outcropping in 10% of the surface (Fig. 2D). In the South, most LURSs developed on 1) dioritic to granitic gneiss, migmatites, while a minor proportion developed on 2) phyllites, mica-schist. Here, the lithologies in which the LURSs developed better match the general distribution of outcrops in that region. The lithologies grouped as "Others" are underrepresented in the LURSs distribution in both regions.

3.2. Current displacement rates of LURSs

Displacement rates have been established for ca. 59% of the 509 LURSs, and from this, ca. 60% (178) show active displacements. The number of active LURSs increases towards the North (Fig. 3; fig. S3). Around 67% of the currently inactive LURSs are located in southern Norway. The proportion of LURSs with displacements slower than 0.5 cm/y is similar throughout Norway. Around 75% of the LURSs with displacements ranging 0.5–1 cm/y are located north of the Polar Circle, as are >79% of those displacing between 1 and 4 cm/y (Fig. 3).

3.3. Past and current permafrost conditions of LURSs

Steep slopes (> 40° on 10 m resolution DEM), represent around 6000 km^2 of cartographic area in Norway. Our model shows that approximately 2700 km^2 of those steep slopes had permafrost (continuous to sporadic) during the LIA. This represents 48% of the steep slopes' surface area (Fig. 4D), meaning that the other 52% already had no permafrost at that time. Our model further shows that 32% of the steep slopes' surface area currently has permafrost, which means that permafrost disappeared in around 16% of the steep slopes between the LIA and now. In Finnmark (Fig. 1), the sporadic permafrost extends down to sea level on coastal cliffs. In southern Norway, the current lower limit is at around 700 m a.s.l. At that altitude, only extremely shaded slopes can have permafrost. The lower modelled altitudinal limit of sporadic permafrost during the LIA was at sea level in northern Norway and ca. 270 m a.s.l. in the south.

From the modelled permafrost during LIA and the location of the LURSs, we observe that during the LIA, a similar number of LURSs existed in permafrost-free and sporadic permafrost areas (Fig. 4A). After the LIA, the reduction in the extent of the permafrost changed the ground conditions of several LURSs. 74 (41 in the South and 33 in the North) of the 197 LURSs that had sporadic permafrost during the LIA, changed to permafrost-free conditions and 65 (15 in the South and 50 in the North) of 101 from discontinuous to sporadic permafrost. Of the 234 LURSs with current permafrost in Norway, ca. 79% are located north of the Polar Circle. Fig. 4A and D show that the proportion of LURSs in the sporadic permafrost class (around 37% at CT) is higher than the proportion of the surface covered by sporadic permafrost (around 21% at CT), which gives a higher number of LURSs per square kilometre in that class (Fig. 4E).

3.4. Controlling factors of displacement rates - Statistical analyses

The relationships between LURSs' volume, lithology, slope, and displacement rates, are presented in Fig. 5. LURSs with smaller volumes seem to have slower displacement rates than the larger ones. However, the pattern is not very clear. Regarding the relation between volume and lithology, we observe that LURSs developed on dioritic to granitic gneiss and migmatites are smaller than those developed on other types of rocks. In addition, at the country scale, LURSs developed on this type of rock seem to present slower displacements. However, this is because this unit is significantly more represented in the South than in the North, where displacement rates are slower. Indeed, a similar relation is not observed when analysing the North and the South separately.

Concerning the relation between current permafrost and displacement rates, LURSs with no permafrost show lower displacement rates than those with permafrost in general (Fig. 6). Sporadic permafrost hosts LURSs with relatively higher displacement rates than discontinuous permafrost (Fig. 6 and fig. S4).

The analysis of minimum MARST shows that displacement rates increase with decreasing temperatures (Fig. 7A). This trend is more evident in northern Norway (Fig. 7B) and more marked in Troms (fig. S5), where the range of temperatures is wider. Currently, inactive LURSs have an average minimum MARST over +3 °C, while it is close to +1 °C for active LURSs.

The analysis of the distribution of permafrost during the LIA and current time (CT), combined with current displacement rates, shows the link between permafrost conditions and the activity of LURSs (Fig. 8; fig. S6). LURSs with permafrost conditions during the LIA are more likely to move than those that did not have permafrost. It is also interesting to

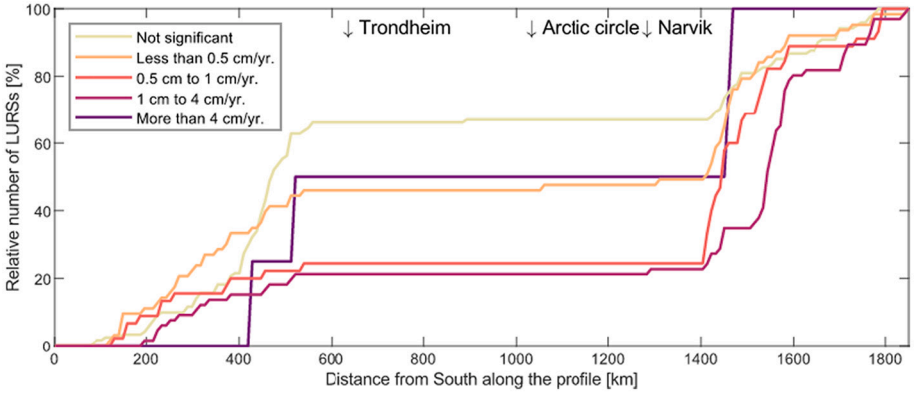

Fig. 3. Cumulative curves of classes of displacement rates from south to north. The location of the LURSs and the profile used to build the cumulative curves are displayed on Fig. 1A.

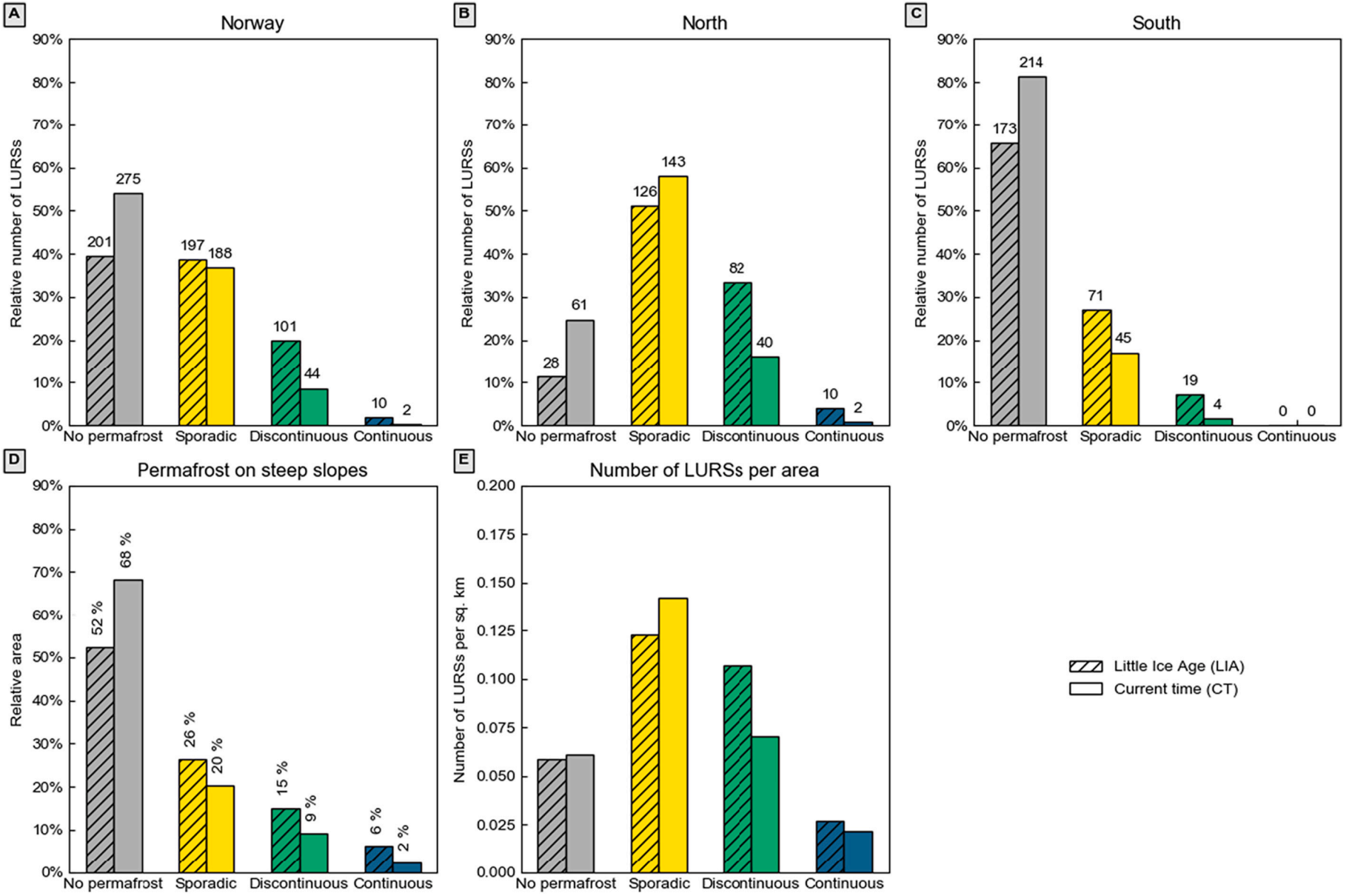

Fig. 4. Temporal change of type of permafrost present in LURSs. A) Histogram showing the proportion of LURSs in each class of permafrost in Norway. B) Histogram showing the proportion of LURSs in each class of permafrost in northern Norway. C) Histogram showing the proportion of LURSs in each class of permafrost in southern Norway. D) Histogram showing the proportion of steep slopes in each class of permafrost. E) Histogram showing the number of LURSs per square kilometre. No permafrost and continuous permafrost are underrepresented in the number of LURSs per square kilometre, while sporadic permafrost and discontinuous permafrost (for the latter mostly in the LIA) are overrepresented.

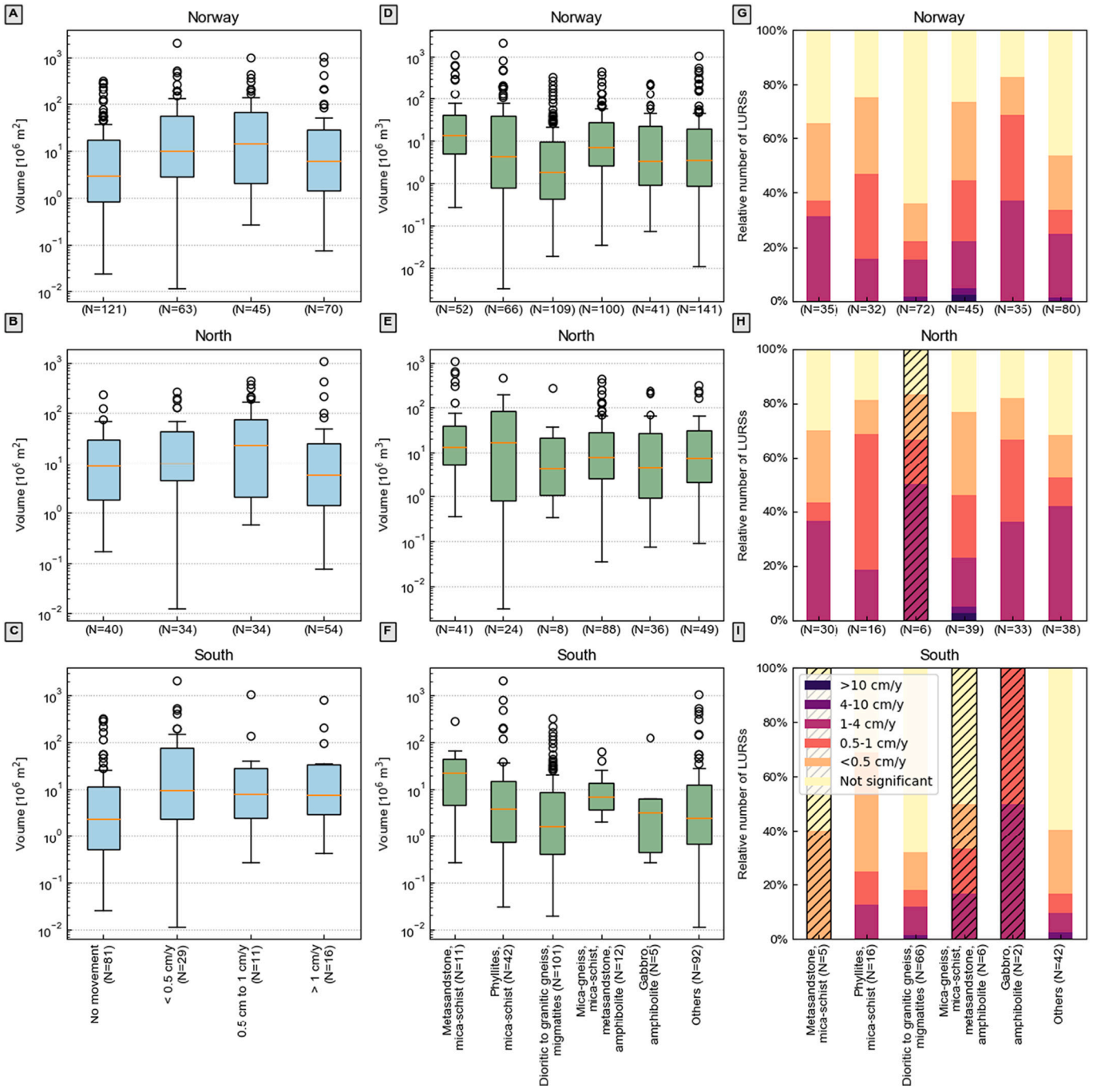

Fig. 5. Boxplots showing the distribution of volumes of LURSs by displacement rate class for the whole country (A), North (B) and South (C) Norway. Box plots showing the distribution of volumes of LURSs by class of lithology for the whole country (D), North (E) and South (F). Stack bars showing the relative distribution of LURSs by lithology and displacement rates classes for the whole country (G), North (H) and South (I). Note: Boxes in boxplot represent 25–75% quartiles and whiskers are 1.5 interquartile ranges from the median. Medians are shown as orange lines. For (G), (H) and (I) where a class represents <10 LURSs, it is shown with a hashed pattern.

observe that the LURSs having discontinuous permafrost during the LIA show less movement if they still have discontinuous permafrost than if they have now sporadic permafrost (Fig. 8). LURSs with no permafrost during the LIA nor in CT are more likely to show no movement or insignificant displacement rates. Globally, ca. 34% of LURSs without permafrost conditions during the LIA are currently moving, while ca. 72% of LURSs with permafrost conditions during the same period show active displacements. 51% of LURSs with permafrost during the LIA but without current permafrost conditions show active displacements, which means that the probability of a LURS being active is 1.6 times higher if the permafrost did not completely thaw between the LIA and CT. These characteristics are visible at the country scale and in the North and South separately (Fig. 8 and fig. S6). Of the 21 LURSs in the South with displacement information, where permafrost thawed completely after the LIA, 10 of them do not show current displacement. Of the 18 LURSs in the North with displacement information where permafrost thawed completely after the LIA, 9 do not show current displacement.

In the results of the statistical tests (Fig. 9), from the values of Kendall's τ, we can observe that the current type of permafrost is positively associated with the displacement rates, although the association is

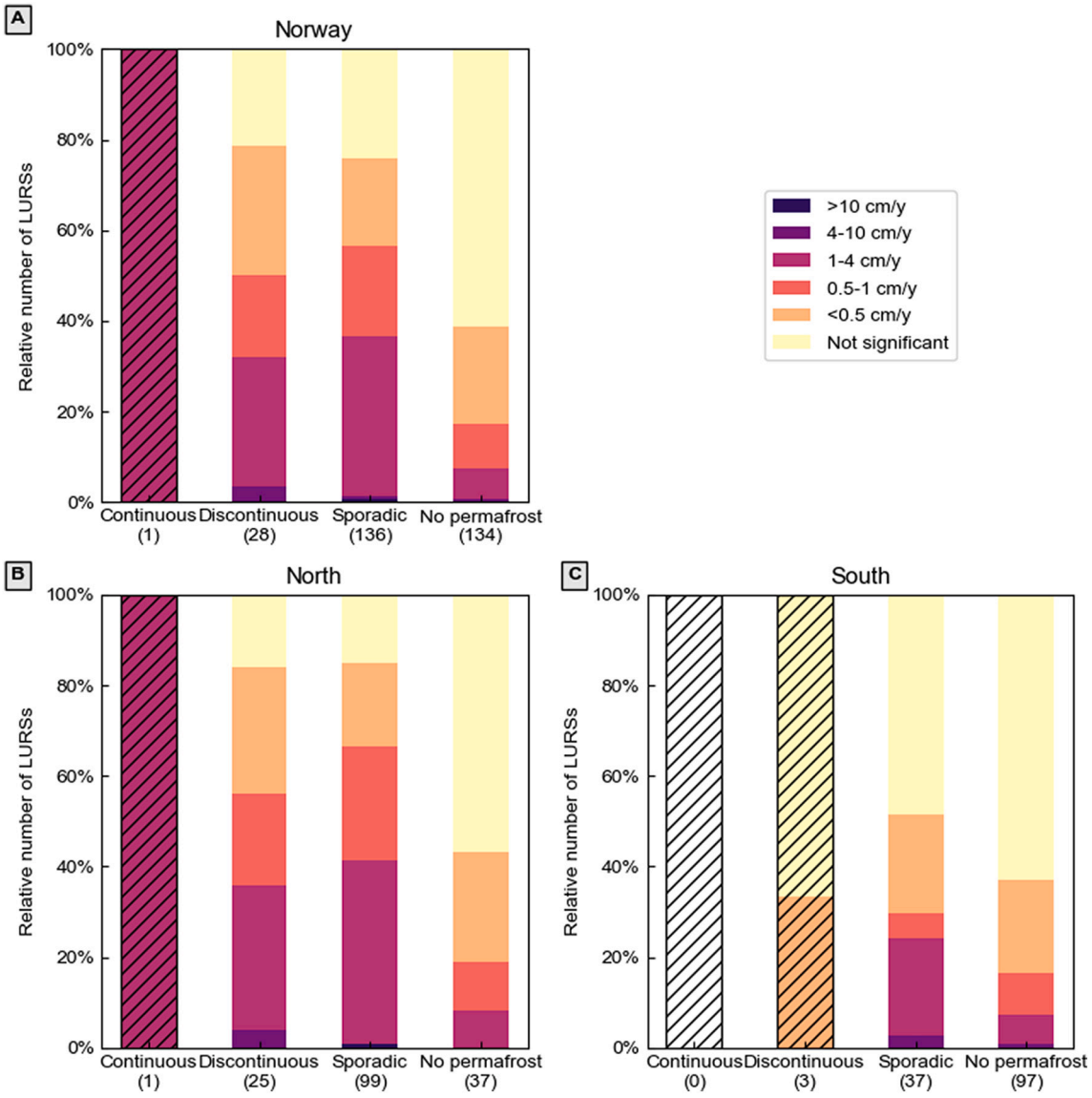

Fig. 6. Stack bar showing the relative distribution of LURSs, the type of permafrost and displacement rate classes for Norway (A), the North (B) and the South (C). Where a class represents <10 LURSs, it is shown with a hashed pattern.

moderate. The association is relatively stable for all geographic areas. It is slightly lower in the South, where permafrost is less widespread (0.13), and has values of 0.30–0.43 for the other regions. The results are statistically significant with *p*-values below 0.01, except for the South where the p-value is not significant (0.1). The association is also positive for the combination of permafrost during the LIA and CT (0.17–0.38), with most p-values below 0.01, except for the South (0.018). The association is negative for the minimum MARST and the displacement rates, meaning lower temperatures correspond with faster displacements. The association is moderate (−0.32 to −0.18), but statistically significant for all regions. On the other hand, the trend is not clear for the association of the volume and the displacement, since τ takes both positive and negative values, and since the associated p-value is significant in only one region (South), partly significant in three other regions (Norway, Troms and Finnmark) and not significant in the last region (North). In the South, the association is the largest (0.20), while the p-value is the lowest, which indicates a positive association between the volume and the displacement rates in this area. This is probably related to the large number of smaller LURSs developed in dioritic to granitic gneiss and migmatites that tend to have not-significant or no displacements. A relatively similar observation can be done for the association between the slope and the displacement rates. At the country scale, the association is negative (−0.13) and statistically significant, meaning LURSs on steeper slopes tend to present less displacement. Similar observations can be made in the South and in Troms, but are only statistically significant in the South. Almost no association is observed when looking at the North, and a positive, but statistically not significant association is observed in Finnmark.

The p-values obtained with the Chi-squared method (Fig. 9) in northern Norway do not show a correlation between lithology and displacement rates. In the South, there is a partial correlation between these parameters. On the other hand, the current permafrost and the displacement rates show a statistical significance for all the regions, except for the South, where the p-value is only partly significant. A similar observation can be made for the combination of permafrost during the LIA and CT in relation to displacement rates, while for this test both the South and the North are only partly significant.

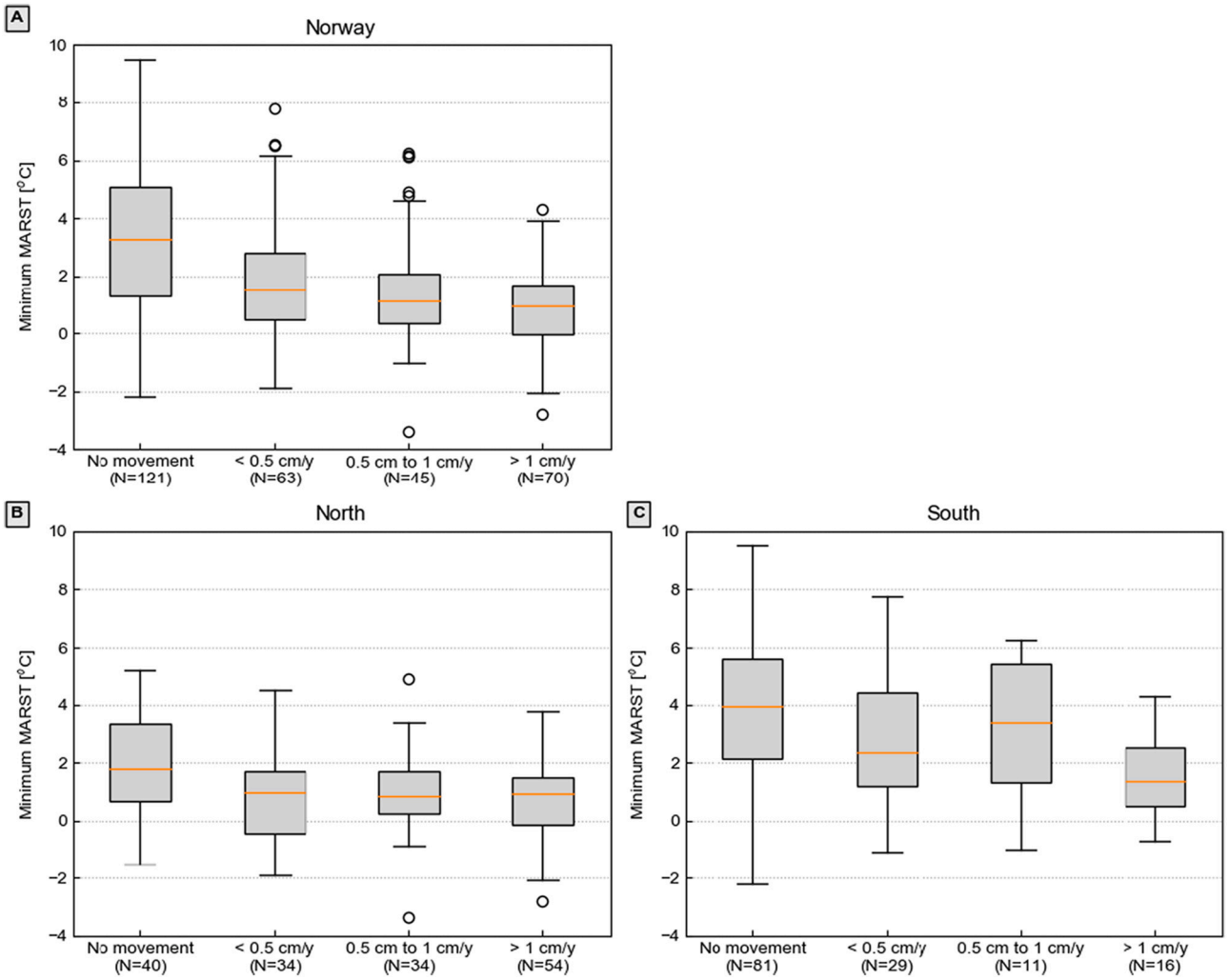

Fig. 7. Boxplots with minimum MARST, and displacement rate classes with amount of LURSs present in each class. Note: Boxes represent 25–75% quartiles and whiskers are 1.5 interquartile ranges from the median. Medians are shown as orange lines.

4. Discussion and conclusions

4.1. Uncertainties and limitations

Two major uncertainties and limitations arise from this study: (1) the statistical evaluation and (2) the co-existence of permafrost and large unstable rock-slopes.

Concerning (1), the Chi-squared and Kendall's τ tests do not differentiate cause-effect from autocorrelation. In our case, we limit the risk of autocorrelation by applying the tests at country-scale, to the North and the South separately and by dividing the North in two. Indeed, since permafrost is mostly present in the North, a correlation with the type of rocks is expected to be seen simply because lithologies are different in the South and the North, while this is less likely inside both regions independently. In addition, we look at different parameters that could explain the difference in displacements, such as size, slope angle, and lithology. Another effect that we do not consider is that Kendall's τ tests test for monotonically increasing or decreasing function. But we see that the relation between permafrost and displacement rates is not monotonical since lower displacement rates are observed and expected where permafrost is either absent or continuous, and higher displacement rates are expected for thawing permafrost (mostly sporadic). However, the low number of LURSs in continuous permafrost implies that we are mainly looking at the discontinuous, sporadic and no permafrost classes.

Concerning (2), the permafrost conditions are based on a temperature map derived statistically and for steady-state conditions. Other processes that are not accounted for in the statistical approach may impact permafrost conditions, such as topographical and transient effects (Noetzli et al., 2007; Noetzli and Gruber, 2009; Myhra et al., 2017). The topographical effects are related to the variable energy balance at the ground surface that is strongly controlled by direct solar radiation, which depends on sun-exposure and latitude. In Norway, the control of the solar radiation on ground surface temperatures is less than in the European Alps (Hipp et al., 2014; Magnin et al., 2019) and induces temperature difference in the order of 2 to 4 °C between north-exposed and south-exposed faces (this decreases with latitude). These differences affect the temperature fields at depth and permafrost that is not expected in a south face when considering statistically-derived surface temperature may exist due to the proximity of a colder north face. This is particularly the case for alpine topography with sharp peaks and spurs. Transient effects that result from the past climatic conditions add to this topographical control. Here again, permafrost may persist at depth even if the predicted permafrost conditions indicate a low probability of its occurrence because of the transient effect of past colder climate. The permafrost map representing current permafrost conditions typically represents conditions for a 30-year period, partially accounting for the recent atmospheric warming (1981–2010). The effect of past and colder decades may persist at depth. In this respect, basing the permafrost classes on permafrost probability limits the risk of misinterpreting the results due to a lack of consideration for past climate because the map

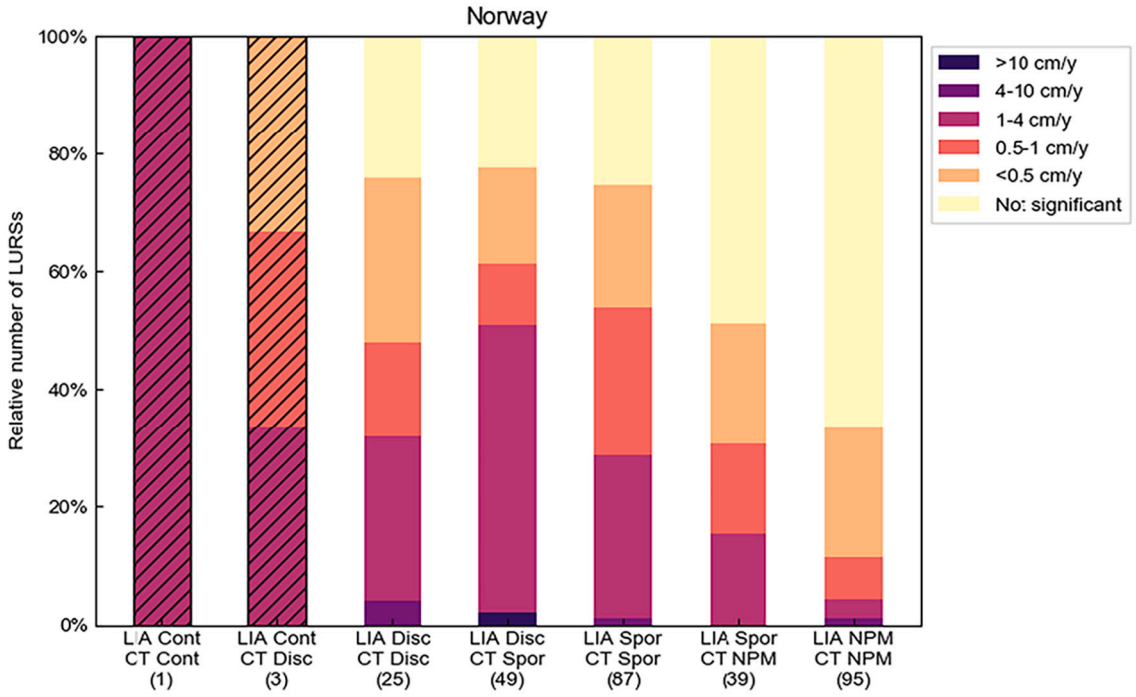

Fig. 8. Stack bar showing the distribution of LURSs by type of permafrost and during the LIA and current times (CT), and classified by current displacement rates. Where a class represents <10 LURSs, it is shown with a hashed pattern. Classes are ordered first by CT permafrost type, then by LIA.

users are made aware that a low probability (e.g. probability falling under the sporadic permafrost class) doesn't necessarily mean the absence of permafrost. Other parameters that may favour the existence of permafrost even under low probability are the snow cover and bedrock fractures. Previous investigations show that permafrost might exist below positive surface temperature up to about 3 °C depending on sun-exposure (Hasler et al., 2011). For example, the Jettan unstable rock-slope in northern Norway, with ice in deep fractures (Blikra and Christiansen, 2014).

4.2. Permafrost and current displacement rates

In Norway, geologic, landscape, and climate conditions control the development of LURSs, their extent and kinematics (Böhme et al., 2013; Booth et al., 2015; Vick et al., 2020). The destabilisation of rock-slopes mainly occurred soon after the Younger Dryas deglaciation, as shown by cosmogenic nuclide dating of sliding surfaces and morphologic assessments (Hermanns et al., 2017; Hilger et al., 2018; Hilger et al., 2021). Differences in precipitation cannot explain differences in displacement rates at country scale. While the mean annual precipitation is higher in the southwest coast (Lussana et al., 2018), the higher displacement rates of LURSs are measured in the North. The fact that the lithologies in which most LURSs developed better match the areal distribution of the lithologies in the South and in the North is primarily due to suitable relief conditions and does not mean LURSs have a higher tendency to develop on a specific lithology. Instead, the high relief areas occupy a larger extension in the South than in the North. Similarly, the lithological units classified as "others" are always underrepresented when considering the LURSs' lithology distribution simply because they are widespread in regions with low relief, where no LURSs developed and have therefore not been differentiated in this analysis. Regarding the activity of the LURSs, a recent study of nine LURSs in northern Norway showed their complex nature and pointed out a link between displacements and structural conditions (Vick et al., 2020). In southern Norway, actively displacing LURSs are mostly seen on phyllites and mica-schist. In four of those LURSs, the poor rock-mass quality was previously proposed as a key control of the active deformation (Böhme et al., 2013; Penna et al., 2017). However, our results show that the correlation between lithologies and displacement rates is only partially significant in the South and not significant in the North. While geologic conditions alone cannot explain the northward increase of displacement rates or even differences in displacement rates in northern Norway, ground temperature variations can. Our results show that permafrost and changes in permafrost co-vary with observed displacement rates, with faster displacement measured in LURSs with a MARST closer to 0 °C suggesting permafrost at depth. This is caused by the cryostatic and hydrostatic changes induced by the warming of permafrost. The factor of safety of ice-filled fractured rocks decreases when ground temperatures get closer to the ice's melting point (Davies et al., 2001); it is equal to 1 or more when ice has fully melted or when temperatures are below the melting point. The shear stress decreases when ice-filled joints warm to temperatures close to 0 °C (Mamot et al., 2021). In addition, the melting of ice increases the water circulation in jointed rocks, enhancing the hydrostatic pressure of the frozen fractured rocks (Murton et al., 2016).

4.3. Permafrost decline and the hazard paradigm

Since the deglaciation of the Fennoscandian Ice Sheet, the permafrost in Norway has undergone drastic variations (Lilleøren et al., 2012). Fluctuations in the extent of permafrost have an impact on the strength of rock-slopes. Recent works discuss how the aggradation and degradation of permafrost undermine their stability (e.g. Voigtländer et al., 2018; Dräbing and Krautblatter, 2019). Our results show that LURSs with discontinuous permafrost during the LIA are more likely to move if they currently have sporadic permafrost than if they currently have discontinuous permafrost. In addition, LURSs with permafrost remaining since the LIA are more likely to move than those with permafrost during the LIA that are currently permafrost-free. This has two main implications; firstly, permafrost degradation can increase displacement rates. This is consistent with the outcomes of recent studies on three LURSs of northern Norway, located on sporadic or discontinuous permafrost, showing that paleo-slip rates were half of the currently measured ones (Böhme et al., 2019; Hilger et al., 2021). Secondly, the complete thaw of permafrost can lead to a decrease in the displacement

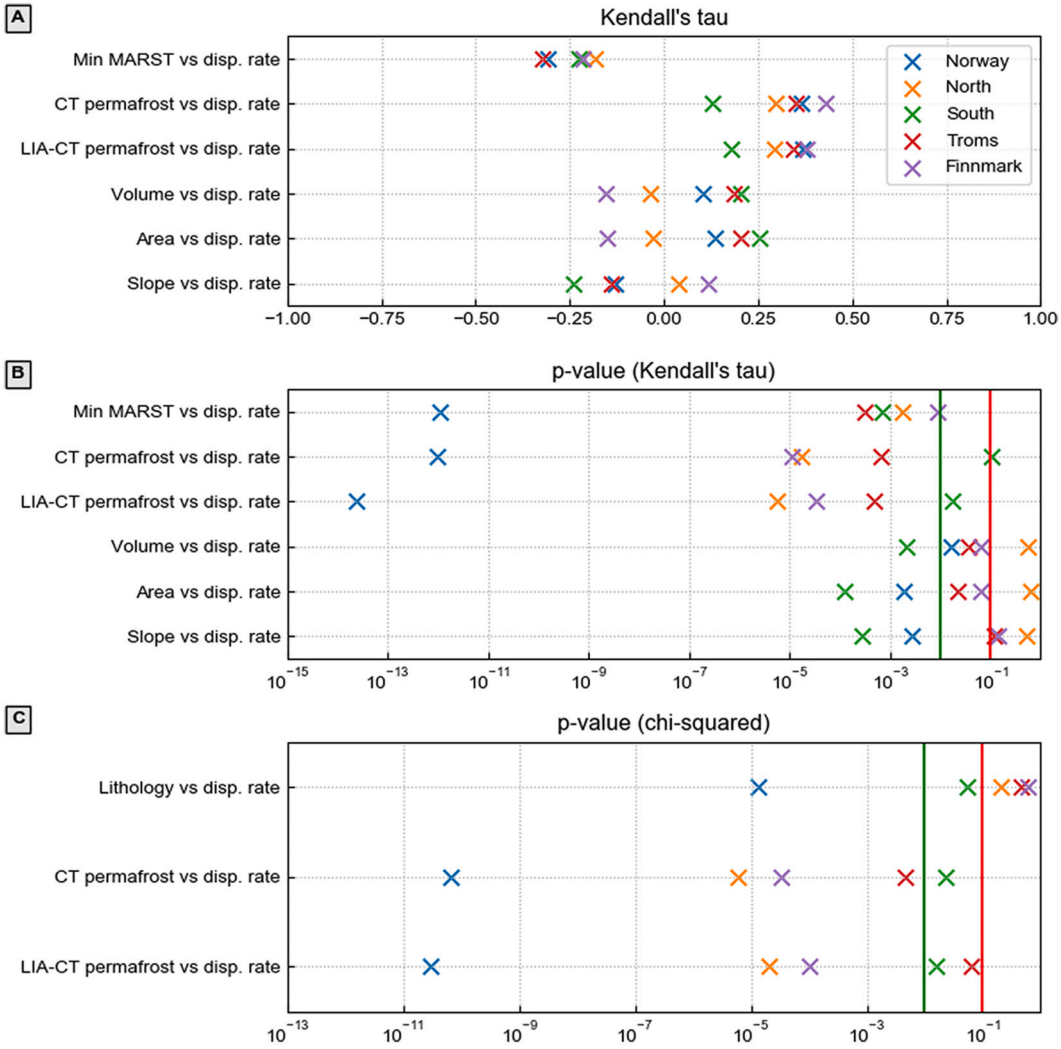

Fig. 9. Results of the statistical tests for different combinations of variables. A) Kendall's τ indicates the association of two variables. A value of 1 indicates a perfect monotonically increasing association, a value of −1 a perfect monotonically decreasing association, and a value of 0 indicates no association. Both p-values (B and C) indicate the statistical significance of the tests, which are considered statistically significant below the green line, partly significant between the green and the red lines and not significant above the red line. Note that permafrost is positively associated with the velocity and the association is statistically significant. On the other hand, volume, area, slope, or rock type are less clearly related to the velocity. (For interpretation of the references to colour in this figure legend, the reader is referred to the web version of this article.)

rates, and LURSs can decelerate until arrest. Both in the North and in the South, half of the LURSs whose permafrost thawed completely after the LIA have insignificant displacement rates or no movement. Therefore, the paradigm of permafrost degradation directly increasing the frequency of failures only partially addresses the effect of ground ice melt associated with the thawing of permafrost. This is because active displacements are often seen as the prelude to failure, and forecasts assume constant external forcing factors. But external factors change with time (Carlá et al., 2017). The formation of a sliding surface requires the nucleation of cracks under appropriate environmental and geologic conditions. As environmental conditions change with time, the development of a sliding surface can be accelerated, deaccelerated, interrupted or reactivated. The complete thaw of permafrost removes the hydrostatic pressure and cryostatic pressure from the rock, leaving the shear force induced by gravity and pre-existing stresses as the main drivers of deformation (Krautblatter et al., 2013). Therefore, if during the period of permafrost and permafrost degradation the accumulated deformation was not enough to drive a slope to failure or to lead to the full development of a sliding surface, a LURS can decelerate and halt (dormant state) once permafrost has completely decayed. However, changes in environmental conditions can drive dormant LURSs to reactivate. In summary, while permafrost warming at temperatures closer to 0 °C can increase the displacement rates of LURSs, thereby increasing the hazard level, the complete thaw of the permafrost can lead to a decrease in their displacements, thereby decreasing the hazard level. However, neither increase nor decrease of displacement rates assures or excludes the possibility of a LURS failing catastrophically.

Author contributions

P,I., Conceptualization, Investigation, Formal Analysis, Writing.
M,F., Conceptualization, Methodology, Formal Analysis, Writing.
N,P., Methodology, Investigation, Formal Analysis, Writing.
E,B., Conceptualization, Writing-reviewing.
H,R.L., Investigation, Supervision.
B,M., Investigation, Writing.
K,L., Investigation, Writing.
N,F., Investigation, Methodology.
B,M., Investigation, Methodology.
D,J.F., Investigation, Methodology.

All authors have read and approved the final manuscript.

Declaration of Competing Interest

None.

Data availability

MARST data for current permafrost analysed during this study are included in Magnin et al. (2019; https://doi.org/10.5194/esurf-7-1019-2019) and its supplementary information files (https://doi.org/10.5194/esurf-7-1019-2019-supplement).

The modelled permafrost map for the Little Ice Age is available from the corresponding author upon request.

InSAR data is freely available at https://insar.ngu.no

The location of LURSs is freely available at https://geo.ngu.no/kart/ustabilefjellparti_mobil/. The polygons used in this study are available from the corresponding author upon request.

Bedrock map available at: https://geo.ngu.no/kart/berggrunn_mobil/

Acknowledgements

The authors acknowledge the Norwegian Water Resources and Energy Directorate for funding most of the research done in the framework of this study. Parts of the study are based on results from the project 'CryoWALL – Permafrost slopes in Norway' (243784/CLE) funded by the Research Council of Norway (RCN) and the University of Oslo, Norway. We would like to express our gratitude to the two anonymous reviewers for their valuable remarks, suggestions and interest in our work.

Appendix A. Supplementary data

Supplementary data to this article can be found online at https://doi.org/10.1016/j.gloplacha.2022.104017.

References

Agresti, A., 2010. Analysis of ordinal categorical data. In: Wiley Series in Probability and Statistics, Second ed. John Wiley & Sons, New York. https://doi.org/10.1002/9780470594001.

Allen, S.K., Gruber, S., Owens, I.F., 2009. Exploring steep bedrock permafrost and its relationship with recent slope failures in the Southern Alps of New Zealand. Permafr. Periglac. Process. 20 (4), 345–356. https://doi.org/10.1002/ppp.658.

Bertolo, D.A., 2017. Decision support system (DSS) for critical landslides and rockfalls and its application to some cases in the Western Italian Alps. Nat. Hazards Earth Syst. Sci. https://doi.org/10.5194/nhess-2017-396. Discuss:1–31.

Biskaborn, B.K., et al., 2019. Permafrost is warming at a global scale. Nat. Commun. 10, 264. https://doi.org/10.1038/s41467-018-08240-4.

Blikra, L.H., Christiansen, H.H., 2014. A field-based model of permafrost-controlled rockslide deformation in northern Norway. Geomorphology. 208, 34–49. https://doi.org/10.1016/j.geomorph.2013.11.014.

Blikra, L.-H., Longva, O., Braathen, A., Anda, E., Dehls, J., Stalsberg, K., 2006. Rock slope failures in Norwegian fjord areas: examples, spatial distribution and temporal pattern. In: Evans, S.G., Mugnozza, G.S., Strom, A., Hermanns, R.L. (Eds.), Landslides from Massive Rock Slope Failure, 49. Springer, Dordrecht. NATO Science Series.

Böhme, M., Hermanns, R.L., Oppikofer, T., Fischer, L., Bunkholt, H.S., Eiken, T., Pedrazzini, A., Derron, M.-H., Jaboyedoff, M., Blikra, L.H., 2013. Analysing complex rock slope deformation at Stampa, western Norway, by integrating geomorphology, kinematics and numerical modeling. Eng. Geol. 154, 116–130.

Böhme, M., Hermanns, R.L., Gosse, J., Hilger, P., Eiken, T., Lauknes, T.R., Dehls, J.F., 2019. Comparison of monitoring data with paleo-slip rates: Cosmogenic nuclide dating detects acceleration of a rockslide. Geology. 47 (4), 339–342. https://doi.org/10.1130/G45684.1.

Booth, A.M., Dehls, J., Eiken, T., Fischer, L., Hermanns, R.L., Oppikofer, T., 2015. Integrating diverse geologic and geodetic observations to determine failure mechanisms and deformation rates across a large bedrock landslide complex: the Osmundneset landslide, Sogn og Fjordane, Norway. Landslides. 12 (4), 745–756. https://doi.org/10.1007/s10346-014-0504-y.

Borradaile, G., 2003. Statistics of Earth Science Data. Springer-Verlag. ISBN 978–3–662-05223-5.

Carlá, T., Intrieri, E., Di Traglia, F., Nolesini, T., Gigli, G., Casagli, N., 2017. Guidelines on the use of inverse velocity method as a tool for setting alarm thresholds and forecasting landslides and structure collapses. Landslides. 14, 517–534. https://doi.org/10.1007/s10346-016-0731-5.

Davies, M.C., Hamza, O., Harris, C., 2001. The effect of rise in mean annual temperature on the stability of rock slopes containing ice-filled discontinuities. Permafr. Periglac. Process. 12, 137–144. https://doi.org/10.1002/ppp.378.

Dehls, J., Larsen, F., Marinkovic, Y., Lauknes, P., Stødle, T.R., Moldestad, D.A., 2019. INSAR.No: a national insar deformation mapping/monitoring service in norway – from concept to operations. In: IGARSS 2019–2019 IEEE International Geoscience and Remote Sensing Symposium, pp. 5461–5464. https://doi.org/10.1109/IGARSS.2019.8898614.

Dräbing, D., Krautblatter, M., 2019. The efficacy of frost weathering processesin Alpine Rockwalls. Geophys. Res. Lett. 46 (12), 6516–6524. https://doi.org/10.1029/2019GL081981.

Etzelmüller, B., Patton, H., Schomacker, A., Czekirda, J., Girod, L., Hubbard, A., Lilleøren, K.S., Westermann, S., 2020. Icelandic permafrost dynamics since the last Glacial Maximum–model results and geomorphological implications. Quat. Sci. Rev. 233, 106236.

Ferretti, A., Prati, C., Rocca, F., 2000. Nonlinear subsidence rate estimation using permanent scatterers in differential SAR interferometry. IEEE Trans. Geosci. Remote Sens. 38 (5), 2202–2212.

Ferretti, A., Prati, C., Rocca, F., 2001. Permanent scatterers in SAR interferometry. IEEE Trans. Geosci. Remote Sens. 39 (1), 8–20.

Fischer, L., Amann, F., Moore, J.R., Huggel, C., 2010. Assessment of periglacial slope stability for the 1988 Tschierva rock avalanche (Piz Morteratsch, Switzerland). Eng. Geol. 116, 32–43. https://doi.org/10.1016/j.enggeo.2010.07.005.

Gisnås, K., Etzelmüller, B., Lussana, C., Hjort, J., Sannel, B., Isaksen, K., Westermann, S., Kuhry, P., Christiansen, H.H., Frampton, A., Åkermann, J., 2016a. Permafrost map for Norway, Sweden and Finland. Permafr. Periglac. Process. 28 (2), 359–378.

Gisnås, K., Westermann, S. Vikhamar, Schuler, T., Melvold, K., Etzelmüller, B., 2016b. Small-scale variation of snow in a regional permafrost model. Cryosphere 10, 1201–1215. https://doi.org/10.1002/ppp.1922.

Gruber, S., Hoelzle, M., Haeberli, W., 2004. Permafrost thaw and destabilisation of Alpine rock walls in the hot summer of 2003. Geophys. Res. Lett. 31, L13504. https://doi.org/10.1029/2004GL020051.

Haeberli, W., Wegmann, M., Vonder Mühll, D., 1997. Slope stability problems related to glacier shrinkage and permafrost degradation in the Alps. Eco. Geol. Helv. 90, 407–414.

Hasler, A., Gruber, S., Haeberli, W., 2011. Temperature variability and offset in steep alpine rock and ice faces. Cryosphere 5, 977–988. https://doi.org/10.5194/tc-5-977-2011.

Hermanns, R., Oppikofer, T., Anda, E., Blikra, L., Böhme, M., Bunkholt, H., Crosta, G., Dahle, H., Devoli, G., Fischer, L., 2012. Recommended Hazard and Risk Classification System for Large Unstable Rock Slopes in Norway: NGU Rapport, 029, p. 53.

Hermanns, R., Blikra, L., Anda, E., Saintot, A., Dahle, H., Oppikofer, T., Fischer, L., Bunkholt, H., Böhme, M., Dehls, J., Lauknes, T., Redfield, T., Osmundsen, P., Eiken, T., 2013. Systematic mapping of large unstable Rock slopes in Norway. In: Margottini, C., Canuti, P., Sassa, K. (Eds.), Landslide Science and Practice. Springer, Berlin Heidelberg, pp. 29–34.

Hermanns, R.L., Schleier, M., Böhme, M., Blikra, L.H., Gosse, J., Ivy-Ochs, S., Hilger, P., 2017. Rock-avalanche activity in W and S Norway Peaks after the retreat of the Scandinavian ice sheet. In: Proceedings Workshop on World Landslide Forum. Springer, pp. 331–338.

Hilger, P., Hermanns, R.L., Gosse, J.C., Jacobs, B., Etzelmüller, B., Krautblatter, M., 2018. Multiple rock-slope failures from Mannen in Romsdal Valley, western Norway, revealed from Quaternary geological mapping and 10Be exposure dating. The Holocene 28 (12), 1841–1854. https://doi.org/10.1177/0959683618798165.

Hilger, P., Hermanns, R., Czekirda, J., Myhra, K.S., Gosse, J., Etzelmüller, B., 2021. Permafrost as a first order control on long-term rock-slope deformation in the (Sub-) Arctic. Quat. Sci. Rev. 251 (1), 106718 https://doi.org/10.1016/j.quascirev.2020.106718.

Hipp, T., Etzelmüller, B., Westermann, S., 2014. Permafrost in Alpine Rock Faces from Jotunheimen and Hurrungane, Southern Norway. Permafr. Periglac. Process. 25, 1–13. https://doi.org/10.1002/ppp.1799.

Hjort, J., Karjalainen, O., Aalto, J., Westermann, S., Romanovsky, V.E., Nelson, F.E., Etzelmüller, B., Luoto, M., 2018. Degrading permafrost puts Arctic infrastructure at risk by mid-century. Nat. Commun. 9 (1), 5147. https://doi.org/10.1038/s41467-018-07557-4.

Huggel, C., Clague, J.J., Korup, O., 2012. Is climate change responsible for changing landslide activity in high mountains? Earth Surf. Process. Landf. 37, 77–91. https://doi.org/10.1002/esp.2223.

Jaboyedoff, M., Carrea, D., Derron, M.-H., Oppikofer, T., Penna, I.M., Rudaz, B., 2020. A review of methods used to estimate initial landslide failure surface depths and volumes. Eng. Geol. 267, 105478 https://doi.org/10.1016/j.enggeo.2020.105478.

Kondratjeva, K.A., Khrutzky, S.F., Romanovsky, N.N., 1993. Changes in the extent of permafrost during the late quaternary period in the territory of the former Soviet Union. Permafr. Periglac. Process. 4 (2), 113–119.

Krautblatter, M., Funk, D., Günzel, F.K., 2013. Why permafrost rocks become unstable: a rock–ice-mechanical model in time and space. Earth Surf. Process. Landf. 38, 876–887. https://doi.org/10.1002/esp.3374.

Kristensen, L., Czekirda, J., Penna, I., Etzelmüller, B., Nicolet, P., Pullarello, J.S., Blikra, L.-H., Skrede, I., Oldani, S., Abellán, A., 2021. Movements, failure and climatic control of the Veslemannen rockslide, Western Norway. Landslides. 18, 1963–1980. https://doi.org/10.1007/s10346-020-01609-x.

Lewkowicz, A.G., Harris, C., 2005. Frequency and magnitude of active-layer detachment failures in discontinuous and continuous permafrost, northern Canada. Permafr. Periglac. Process. 16, 115–130. https://doi.org/10.1002/ppp.522.

Lewkowicz, A., Way, R.G., 2019. Extremes of summer climate trigger thousands of thermokarst landslides in a High Arctic environment. Nat. Commun. 10, 1329. https://doi.org/10.1038/s41467-019-09314-7.

Liljedahl, A.K., et al., 2016. Pan-Arctic ice-wedge degradation in warming permafrost and its influence on tundra hydrology. Nat. Geosci. 9, 312–318. https://doi.org/10.1038/ngeo2674.

Lilleøren, K., Etzelmüller, B., Schuler, V.T., Gisnås, K., Humlum, O., 2012. The relative age of mountain permafrost — estimation of Holocene permafrost limits in Norway. Glob. Planet. Chang. 92-93, 209–223. https://doi.org/10.1016/j.gloplacha.2012.05.016.

Lussana, C., Saloranta, T., Skaugen, T., Magnusson, J., Tveito, O.E., Andersen, J., 2018. seNorge2 daily precipitation, and observational gridded dataset over Norway from 1957 to the present day. Earth Syst. Sci. Data. 10, 235–249.

Magnin, F., Etzelmüller, B., Westermann, S., Isaksen, K., Hilger, P., Hermanns, R.L., 2019. Permafrost distribution in steep rock slopes in Norway: measurements, statistical modelling and implications for geomorphological processes. Earth Surf. Dynam. 7, 1019–1040. https://doi.org/10.5194/esurf-7-1019-2019.

Mamot, P., Weber, S., Schröder, T., Krautblatter, M., 2018. A temperature- and stress-controlled failure criterion for ice-filled permafrost rock joints. Cryosphere 12, 3333–3353. https://doi.org/10.5194/tc-12-3333-2018.

Mamot, P., Weber, S., Eppinger, S., Krautblatter, M., 2021. A temperature-dependent mechanical model to assess the stability of degrading permafrost rock slopes. Earth Surf. Dyn. 9, 1125–1151. https://doi.org/10.5194/esurf-9-1125-2021.

Massonnet, D., Feigl, K.L., 1998. Radar interferometry and its application to changes in the Earth's surface. Rev. Geophys. 36, 441–500. https://doi.org/10.1029/97RG03139.

Murton, J., Kuras, O., Krautblatter, M., Cane, T., Tschofen, D., Uhlemann, S., Schober, S., Watson, P., 2016. Monitoring rock freezing and thawing by novel geoelectrical and acoustic techniques. J. Geophys. Res. 121, 2309–2332. https://doi.org/10.1002/2016JF003948.

Myhra, K.S., Westermann, S., Etzelmüller, B., 2017. Modelled distribution and Temporal Evolution of Permafrost in Steep Rock Walls along a Latitudinal Transect in Norway by CryoGrid 2D. Permafr. Periglac. Process. 28, 172–182. https://doi.org/10.1002/ppp.1884.

Noetzli, J., Gruber, S., 2009. Transient thermal effects in Alpine permafrost. Cryosphere 3, 85–99. https://doi.org/10.5194/tc-3-85-2009.

Noetzli, J., Gruber, S., Kohl, T., Salzmann, N., Haeberli, W., 2007. Three-dimensional distribution and evolution of permafrost temperatures in idealized high-mountain topography. J. Geoph. Res. 112 https://doi.org/10.1029/2006JF000545.

Obu, J., Westermann, S., Bartsch, A., Berdnikov, N., Christiansen, H.H., Dashtseren, A., Delaloye, R., Elberling, B., Etzelmüller, B., Kholodov, A., 2019. Northern Hemisphere permafrost map based on TTOP modelling for 2000–2016 at 1 km2 scale. Earth Sci. Rev. 193, 299–316. https://doi.org/10.1016/j.earscirev.2019.04.023.

Oppikofer, T., Nordahl, B., Bunkholt, H., Nicolaisen, M., Jarna, A., Iversen, S., Hermanns, R.L., Böhme, M., Molina, F.X.Y., 2015. Database and online map service on unstable rock slopes in Norway—from data perpetuation to public information. Geomorphology. 249, 69–81. https://doi.org/10.1016/j.geomorph.2015.08.005.

Oppikofer, T., Böhme, M., Nicolet, P., Penna, I., Hermanns, R.L., 2016. Metodikk for Konsekvensanalyse av Fjellskred. Norges Geologiske Undersøkelse. Available at. http://www.ngu.no/upload/Publikasjoner/Rapporter/2016/2016_047.pdf.

Pearson, K., 1900. On the criterion that a given system of deviations from the probable in the case of a correlated system of variables is such that it can be reasonably supposed to have arisen from random sampling. The London, Edinburgh and Dublin Phil Mag J Sci Ser. 5 (50), 157–175.

Penna, I., Böhme, M., Hermanns, R.L., Eiken, T., Dehls, J., 2017. Large-scale rockslope deformations in Sogn Og Fjordane County (Norway). In: Mikoš, M., Casagli, N., Yin, Y., Sassa, K. (Eds.), Advancing Culture of Living with Landslides. World Landslide Forum 2017. Springer International Publishing, Cham, pp. 601–606.

Phillips, M., Wolter, A., Lüthi, R., Amann, F., Kenner, R., Bühler, Y., 2017. Rock slope failure in a recently deglaciated permafrost rock wall at Piz Kesch (Eastern Swiss Alps), February 2014. Earth Surf. Process. Landf. 42, 426–438. https://doi.org/10.1002/esp.3992.

Ravanel, L., Deline, P., 2011. Climate influence on rockfalls in high-Alpine steep rockwalls: the north side of the Aiguilles de Chamonix (Mont Blanc massif) since the end of the 'Little Ice Age'. The Holocene 21 (2), 357–365. https://doi.org/10.1177/0959683610374887.

Ravanel, L., Magnin, F., Deline, P., 2017. Impacts of the 2003 and 2015 summer heatwaves on permafrost-affected rock-walls in the Mont Blanc massif. Sci. Total Environ. 609, 132–143. https://doi.org/10.1016/j.scitotenv.2017.07.055.

Shugar, D., et al., 2021. A massive rock and ice avalanche caused the 2021 disaster at Chamoli. Indian Himal. Sci. 373 (6552), 300–306. https://doi.org/10.1126/science.abh4455.

Svennevig, K., Dahl-Jensen, T., Keiding, M., Merryman Boncori, J.P., Larsen, T.B., Salehi, S., Munck Solgaard, A., Voss, P.H., 2020. Evolution of events before and after the 17 June 2017 rock avalanche at Karrat Fjord, West Greenland – a multidisciplinary approach to detecting and locating unstable rock slopes in a remote Arctic area. Earth Surf. Dynam. 8 (4), 1021–1038. https://doi.org/10.5194/esurf-8-1021-2020.

Swindles, G.T., et al., 2015. The long-term fate of permafrost peatlands under rapid climate warming. Nat. Sci. Rep. 5, 17951. https://doi.org/10.1038/srep17951.

Vick, L.M., Böhme, M., Rouyet, L., Bergh, S.G., Corner, G.D., Lauknes, T.R., 2020. Structurally controlled rock slope deformation in northern Norway. Landslides. 17, 1745–1776. https://doi.org/10.1007/s10346-020-01421-7.

Voigtländer, A., Leith, K., Krautblatter, M., 2018. Subcritical crack growth and progressive failure in Carrara marble under wet and dry conditions. J. Geophys. Res. Solid Earth 123 (5), 3780–3798. https://doi.org/10.1029/2017JB014956.

Wasowski, J., Bovenga, F., 2014. Investigating landslides and unstable slopes with satellite Multi Temporal Interferometry: current issues and future perspectives. Eng. Geol. 174, 103–138. https://doi.org/10.1016/j.enggeo.2014.03.003.